JOURNAL OF ELECTROMAGNETIC ENGINEERING AND SCIENCE, VOL. 23, NO. 1, 47~56, JAN. 2023

https://doi.org/10.26866/jees.2023.1.r.143
ISSN 2671-7263 (Online) · ISSN 2671-7255 (Print)

A Wideband Ultra-Low-Profile Solar Cell–Integrated Antenna

Ahmed Ali[1] · Heesu Wang[1] · Yeojun Yun[1] · Sungjun Park[1] · Yong Bae Park[1,2] · Jaejin Lee[1] · Ikmo Park[1,*]

Abstract

In this paper, a wideband ultra-low-profile solar cell–integrated antenna with a high form factor is presented. A copper indium gallium selenide-based solar cell was used for the proposed design. The solar cell was cut with a rectangular-shaped narrow slit to construct a built-in solar cell antenna with dimensions of 50 mm × 20 mm × 0.571 mm ($0.382\lambda_o \times 0.152\lambda_o \times 0.0043\lambda_o$ at 2.28 GHz). The slit area needed to achieve a high form factor was only 0.5 mm × 18 mm. A coaxial-to-microstrip-line transition type of feeding structure was used to excite the antenna. An RF decoupler circuit was also designed under the second substrate to maintain the independent functioning of both devices. The simulated and measured results are in good agreement. Furthermore, the proposed design demonstrated a –10 dB impedance bandwidth of 42.45% with an ultra-low-profile structure of $0.0043\lambda_o$ at 2.28 GHz, and the maximum gain was 2.84 dBi in the impedance bandwidth range. In addition, the antenna has a high form factor of 99.1%, with no optical blockage.

Key Words: Integrated Antenna, IoT Devices, Solar Cell, Slit Antenna, Ultra-Low-Profile Antenna, Wideband Antenna.

I. INTRODUCTION

Antennas play a fundamental role in wireless communication systems. In recent years, different types of antennas have been developed to enhance the overall performance of communication systems. Advancements in modern wireless communication systems and their increasing applications require compact, broadband, and high-efficiency antennas [1, 2]. Moreover, the demand for multifunctional antennas is increasing due to the impact of the Internet of Things (IoT) and wireless sensor network (WSN) applications [3]. In addition, multifunctional devices have become very popular for the miniaturization of communication systems [4, 5]. In this context, a solar cell–integrated antenna is a good option for an autonomous communication system. The integration of solar cells with antennas results in a self-sustained communication system that does not require an additional power supply, and these communication devices can be used in remote locations.

Various approaches and techniques have been used to integrate antennas and solar cells into a single dual-function device [6–13]. When integrating solar cells with antennas, the two devices must be compatible, and they must not affect each other. Solar cells have been integrated with slit [14], patch [15], substrate integrated waveguide [16], crossed-dipole [17], reflectarray [18], and inverted-F [19] antennas. Using solar cells as radiators has recently received much attention from several research groups [20–22]. Some researchers have presented a solar cell–integrated antenna in which the solar cell is also used as a ground plane for the antenna [23, 24]. This design approach helps decrease the antenna's overall size. Transparent materials

Manuscript received May 11, 2022 ; Revised August 30, 2022 ; Accepted October 19, 2022. (ID No. 20220511-066J)
[1]Department of Electrical and Computer Engineering, Ajou University, Suwon, Korea.
[2]Department of AI Convergence Network, Ajou University, Suwon, Korea.
[*]Corresponding Author: Ikmo Park (e-mail: ipark@ajou.ac.kr)

are used in the antenna design to increase the optical transparency of the solar cells [25] and are placed at the top of the solar cell to design a solar cell–integrated antenna. However, an optically transparent antenna has limited use due to its complex manufacturing process and high cost. Mesh-type antennas are also good candidates for solar cell–integrated antennas because they can be directly designed by placing them at the top of the solar cell [26]; however, this placement reduces the optical transparency for the solar cell.

Another method was proposed by Ali et al. [27], in which a slit is etched from the solar cell, resulting in a low-profile solar cell built-in antenna. The slit used for the design occupies approximately 10% of the total solar cell–integrated antenna area, which reduces the effective area of solar cells, thus decreasing the solar cell conversion efficiency. To solve this problem, the ground radiation antenna method, in which a small slit is etched from a solar cell, has also been used. Although using a small slit increases the solar cell's effective area, the design has only a 5% impedance bandwidth [28]. Moreover, the design complexity level increases due to the use of lumped elements in ground radiation antennas. It was noticed in previous solar cell–integrated antennas that either the solar cell characteristics or the antenna characteristics were compromised when integrating both devices. In addition, researchers have noted that when the ratio of the solar cell area to the total antenna area is very low, it eventually decreases the form factor in solar cell–integrated antennas. Therefore, it is necessary to design a solar cell–integrated antenna that possesses high optical transparency, a high form factor, a low-profile structure, a simple design with a wide impedance bandwidth, and good radiation characteristics.

In this paper, we propose an ultra-low-profile solar cell–integrated antenna with a wide impedance bandwidth and a high form factor. An ultra-low-profile copper indium gallium selenide (CIGS)-based solar cell is used in the design. A very thin slit is cut from the solar cell. The advantage of using a narrow slit is that only a very small area is used for the antenna operation, which maximizes the area of the solar cell that can be utilized for power generation. Thus, the proposed solar cell–integrated antenna has a high form factor, and the proposed design has a wide impedance bandwidth of 42.45%, with good radiation characteristics in terms of the antenna features.

II. Configuration of the Solar Cell Built-in Antenna

The proposed antenna configuration is depicted in Fig. 1. A 3D view of the solar cell–integrated antenna, top view of the solar cell–integrated antenna, top view of the bottom contact of the solar cell with the slit, bottom view of the solar cell–integrated antenna, and side view are shown in Fig. 1(a)–1(e), respectively.

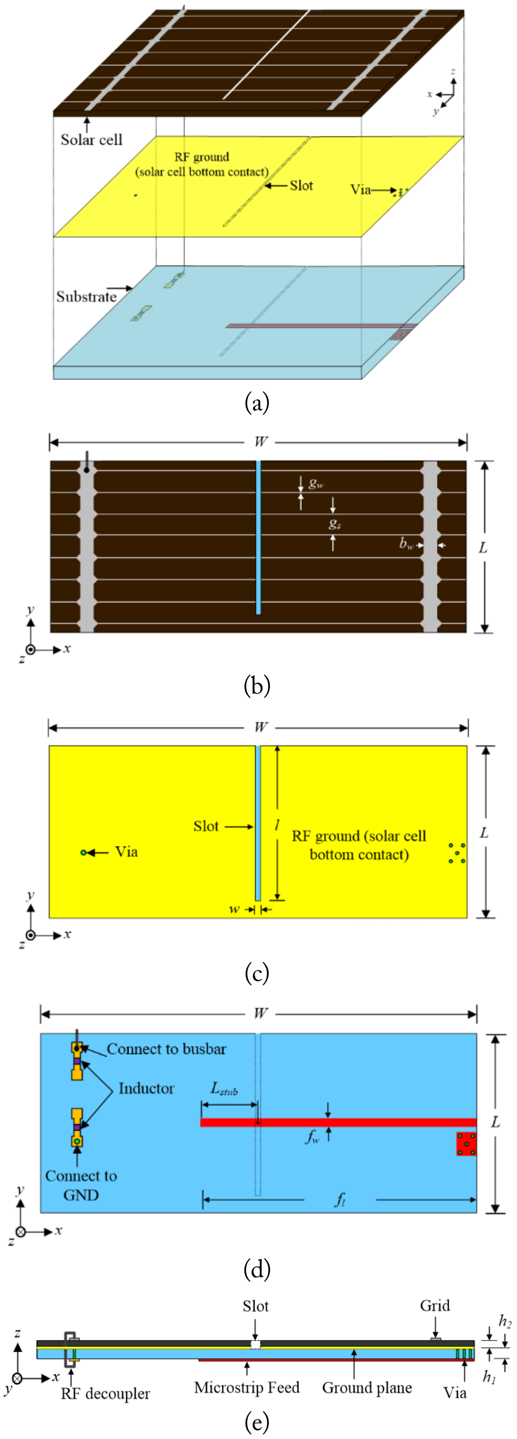

Fig. 1. Detailed geometry of the solar cell–integrated antenna: (a) 3D view, (b) top view, (c) top view of the bottom contact of the solar cell with the slit, (d) top view of the bottom side, and (e) side view.

An ultra-low-profile CIGS-based solar cell is integrated with the antenna. The solar cell's dimensions are $W \times L \times h_1$, and the cell itself consists of three layers. The top layer is composed of metallic grids and busbars. The width of each grid is 0.001 mm, and there is a distance of 1.5 mm between the grids. Busbars were designed to collect power. Each busbar is 1.5 mm wide, and they are 20 mm apart. Under the metallic grids and busbars is the second layer of the solar cell, which is made of copper, indium, gallium, and selenide. The total thickness of the second layer is only 0.004 mm. The third layer is the bottom metallic contact. Stainless steel is used, and it is 0.059 mm. The ANSYS High-Frequency Structure Simulator (HFSS), an electromagnetic wave simulator based on the finite element method, was used to conduct numerical simulations that analyzed the performance of the proposed solar cell with the built-in antenna design. A single layer of a 0.059 mm thick dielectric with a dielectric constant of 12.9 and a loss tangent of 0.0064 was used to model the CIGS solar cell in the EM simulator.

An open-ended slit was cut from the solar cell to design an integrated balun structure. This slit was cut from all the layers of the solar cell because of the solar cell's conductivity. It is well-known that the conductivity of the solar cell is due to the p-n junction formed by doping, so that cutting all the layers results in a low-profile solar cell–integrated antenna. However, the existence of the slit also reduces the effective area of the solar cell because some of its parts cannot be used to generate power. Because of this limitation, a very narrow slit of only 0.5 mm × 18 mm was used to achieve a high form factor. A coaxial-to-microstrip-line transition type of feeding structure was used to excite the antenna through the slit. The solar cell's bottom metallic contact is also used as the ground plane for the antenna. A small metallic patch is used alongside the microstrip feedline, which is connected to the bottom metallic contact of the solar cell using via holes. Another substrate is used under the solar cell to design a microstrip feedline and a small metallic patch. The second substrate is 0.508 mm, while the dielectric constant and the loss tangent are 3.38 and 0.0027, respectively.

An RF decoupler circuit was added to the proposed design so that the solar cells and the antenna function independently of each other. For the RF decoupler circuit, two metallic traces were designed under the second substrate. Two inductors were used as an RF choke, and they were inserted inside the metallic traces. The dimensions of each inductor are 1 mm × 1 mm, and both have an inductance of 56 nH. During the simulation, the inductors were modeled as lumped elements. The inductance value varied from 30 nH to 70 nH, and it was discovered that varying the inductance value had a negligible effect on the antenna performance. Busbars were used to collect power from the solar cell. The busbar is connected with the metallic trace using a connecting wire, while the second patch is connected to the bottom contact of the solar cell using a via hole. The final design parameters of the solar cell–integrated antenna are $W = 50$ mm, $L = 20$ mm, $h_1 = 0.063$ mm, $h_2 = 0.508$ mm, $l = 18$ mm, $w = 0.5$ mm, $f_w = 1.2$ mm, $f_l = 33$ mm, $b_w = 1.5$ mm, $g_w = 0.1$ mm, $L_{stub} = 8$ mm, and $g_s = 1.5$ mm.

III. Operational Mechanism

Detailed studies have been conducted to analyze the operational mechanism of the proposed wideband solar cell–integrated antenna. The two resonances are generated using an integrated balun structure, which consists of a narrow slit and a microstrip feedline. The input impedances in terms of the real and imaginary parts are shown in Fig. 2. It can be seen from the figure that when the length of the slit increases, the input impedance decreases. Changing the slit length does not have an effect on the gain characteristics, as shown in Fig. 3.

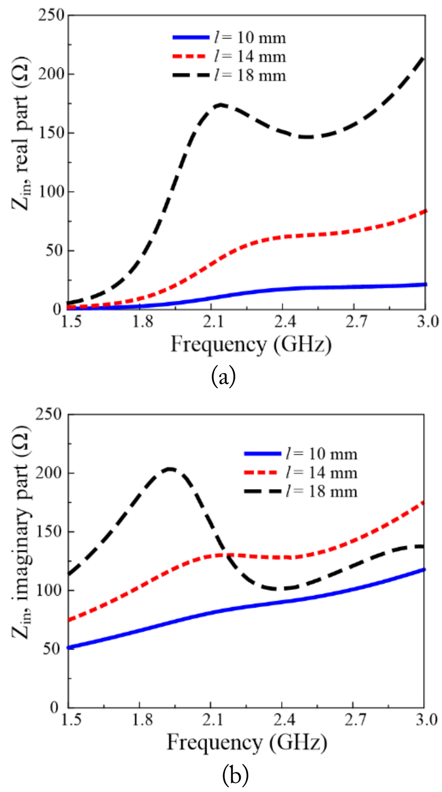

Fig. 2. Impedance of the proposed ground slit antenna with varying slit lengths: (a) the real part and (b) the imaginary part.

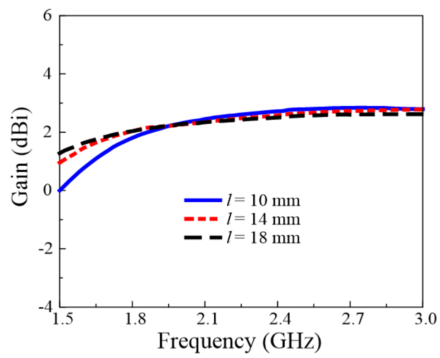

Fig. 3. Gain of the proposed ground slit antenna with varying slit lengths.

The radiation mechanism of the proposed structure is similar to that of a conventional loop antenna. A conventional loop antenna can be described as a two-element dipole array. The x-axis arms work as a dipole element, while the y-axis arms work as a phase-delay line. To verify this, a conventional loop antenna was studied, and the radiation characteristics were compared with the proposed design. The structure of the conventional loop antenna and the proposed ground slit antenna is shown in Fig. 4. The radiation mechanism of the conventional loop antenna and the proposed antenna is compared in Fig. 5. It is shown in the figure that the proposed design works as a two-element dipole array. The radiation patterns of the conventional loop antenna and the proposed ground slit antenna are similar, as shown in Fig. 6.

The surface current distribution of the proposed design was also examined to analyze the radiation mechanism. The surface current distribution at 1.98 GHz and 2.52 GHz is shown in Fig. 7. The current intensity is visible at two dipole elements that result in radiation.

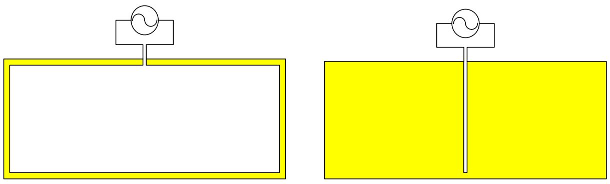

(a) (b)

Fig. 4. Structure of (a) the conventional loop antenna and (b) the proposed ground slit antenna.

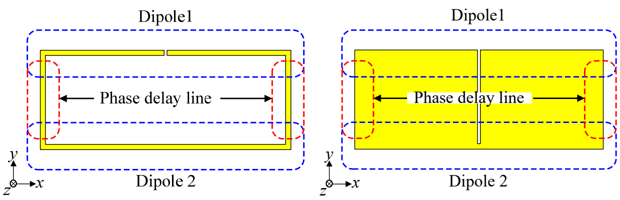

(a) (b)

Fig. 5. Radiation mechanism of (a) the conventional loop antenna and (b) the proposed ground slit antenna.

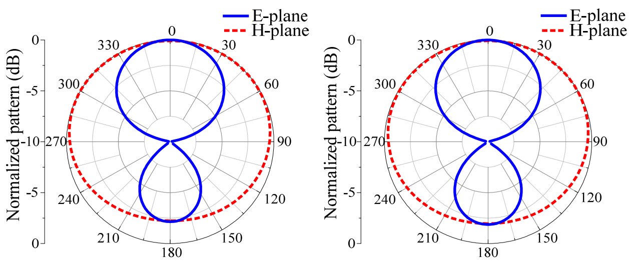

(a) (b)

Fig. 6. Radiation patterns of (a) the conventional loop antenna and (b) the proposed ground slit antenna.

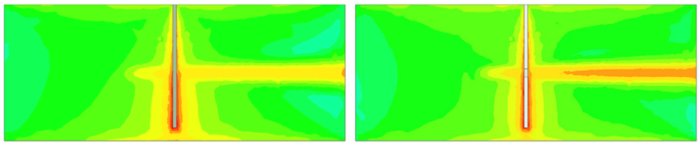

(a) (b)

Fig. 7. Surface current distribution of the proposed antenna: (a) 1.9 GHz, and (b) 2.5 GHz.

IV. Simulation Results and Discussion

The HFSS was used for all simulations, as well as optimization. The length and width of the slit were optimized so that the smallest possible area was used. The key parameters of the proposed solar cell–integrated antenna were chosen according to parametric analysis and understanding of the operational mechanism. During parametric analysis, one parameter was varied, while all other parameters were unchanged. In Fig. 8, the effect of varying the slit's length is shown. The slit length is critical for controlling the resonance frequency, and the resonance frequency shifted toward the lower frequency band as the slit length increased from 17 mm to 19 mm. The optimal value used for the slit length was 18 mm. The effect of varying the slit width on the reflection coefficient is presented in Fig. 9. As can be seen in this figure, the slit width varies from 0.1 mm to 0.5 mm. Decreasing the slit width from 0.5 mm to 0.1 mm worsened the

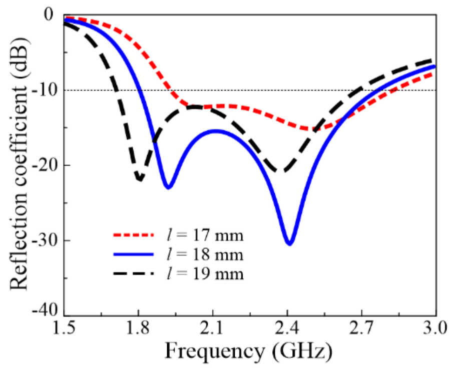

Fig. 8. Reflection coefficients with varying slit lengths.

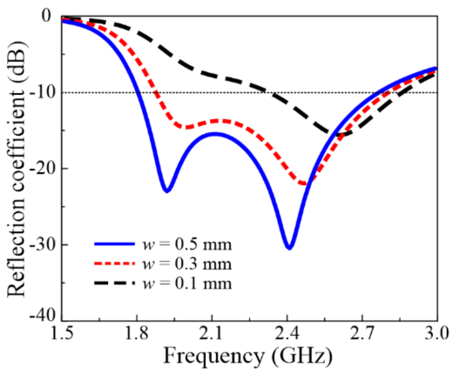

Fig. 9. Reflection coefficients with varying slit widths.

impedance matching, and it was noted that the resonance frequency remained unchanged when the slit width varied. Then, the effect of the microstrip feedline's length and width was investigated. The effect of the length of the feedline f_l on the reflection coefficient is shown in Fig. 10. For the analysis, the feedline's length varied from 32 mm to 34 mm. It is apparent from the figure that increasing the value of f_l improves the impedance matching, but the impedance bandwidth decreases. The optimum value for f_l is 33 mm, which achieves a broader bandwidth with good impedance matching. When the effect of f_l was examined, it was noticed that the feeding position P_{feed} and the distance from the end of the feedline to the feeding position where the feedline sees the aperture L_{stub} are also very important. The feedline was moved across the slit to analyze the effect of P_{feed}, as shown in Fig. 11. Increasing the P_{feed} has a significant effect on the real and imaginary parts of the impedance, as shown in Fig. 12. When P_{feed} is zero, the real and imaginary parts of the impedance are very high, but increasing the P_{feed} decreases the impedance. The optimum value chosen for P_{feed} is 10 mm, where the real part of the impedance is close to 50 Ω. To examine the effect of L_{stub}, L_{stub} was changed from 4 mm to 12 mm. The optimum value chosen for L_{stub} was 8 mm. The real part of the impedance decreased significantly when L_{stub} was changed to 4 mm and 12 mm, as shown in Fig. 13. However, the imaginary part of the impedance decreased when L_{stub} was increased, as shown in the figure. The effect of varying L_{stub} on the gain characteristics is presented in Fig. 14. It is obvious from the figure that varying L_{stub} has almost no effect on the gain within the impedance bandwidth.

The width of the feedline f_w also has a significant effect on the reflection coefficient of the proposed solar cell–integrated antenna, as shown in Fig. 15. The effect of f_w on the reflection coefficient was analyzed using 0.8 mm, 1.0 mm, and 1.2 mm. When f_w decreases, the impedance bandwidth increases, but the impedance matching over the impedance bandwidth is degraded.

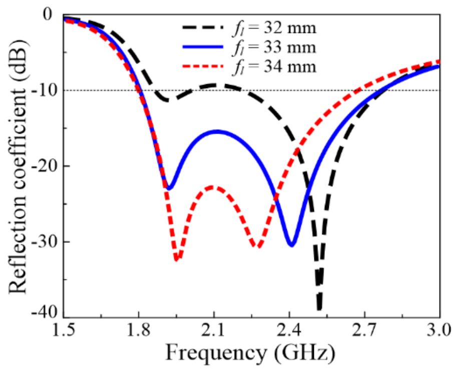

Fig. 10. Reflection coefficients with varying feedline lengths.

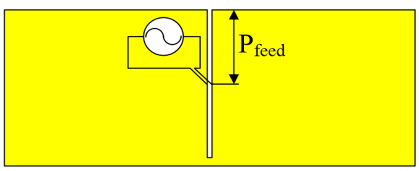

Fig. 11. Varying P_{feed} across the slit.

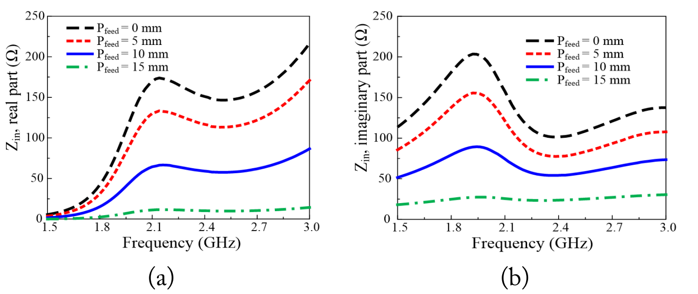

Fig. 12. Impedance of the proposed ground slit antenna with varying P_{feed}: (a) the real part and (b) the imaginary part.

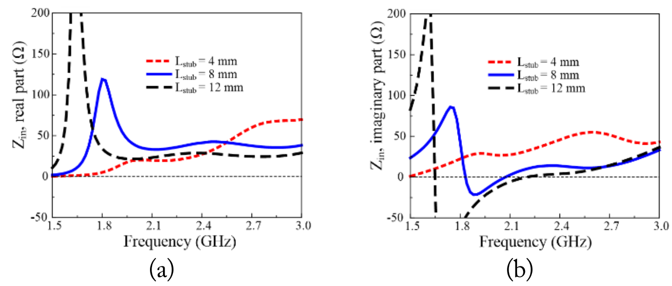

Fig. 13. Impedance of the proposed ground slit antenna with varying L_{stub}: (a) the real part and (b) the imaginary part.

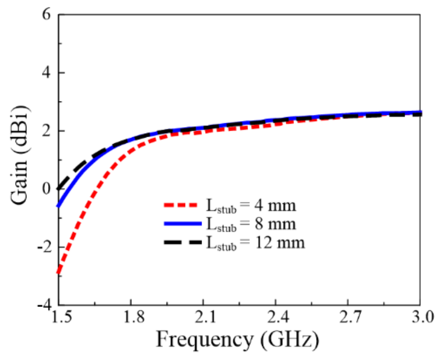

Fig. 14. Gain characteristics when L_{stub} is changed.

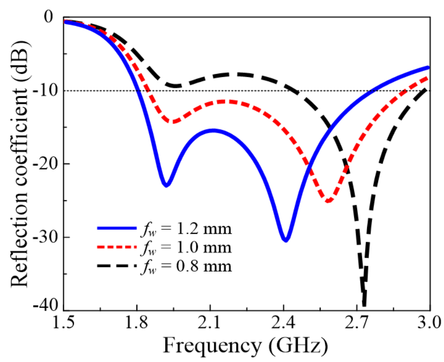

Fig. 15. Reflection coefficients with varying feedline widths.

The optimum value selected for f_w is 1.2 mm.

Additionally, the number and width of the gridlines were varied to examine the effect of the solar cell on the antenna's performance. The number of gridlines on the solar cell and their width had a negligible effect on the antenna's performance, as shown in Figs. 16 and 17. The performance of the solar cell in terms of the I–V and power curve characteristics was also analyzed with and without cutting a slit in the solar cell. It was noticed that cutting a slit in the solar cell had a negligible effect on the solar cell performance, as shown in Figs. 18 and 19. The proposed design shows a wide fractional impedance bandwidth of 42.45%, which ranges from 1.80 GHz to 2.77 GHz, while the gain varies from 2.38 dBi to 2.70 dBi in the impedance bandwidth range. A comparison of the proposed solar cell–integrated antenna with existing solar cell antennas is shown in Table 1. It is evident from the table that the proposed design has a broader impedance bandwidth while maintaining a low-profile structure and achieving a high form factor.

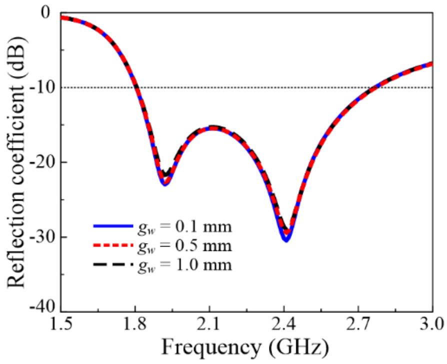

Fig. 16. Reflection coefficients with varying gridline widths.

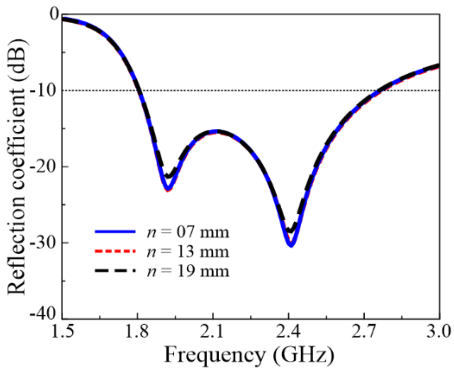

Fig. 17. Reflection coefficients with different gridline numbers.

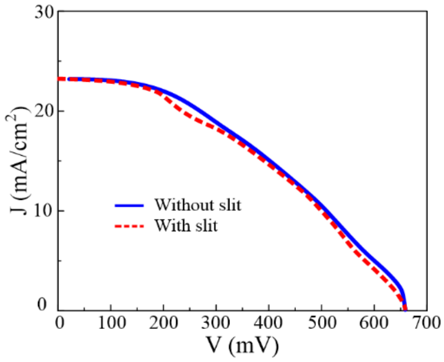

Fig. 18. I-V curve characteristics of solar cell with and without slit.

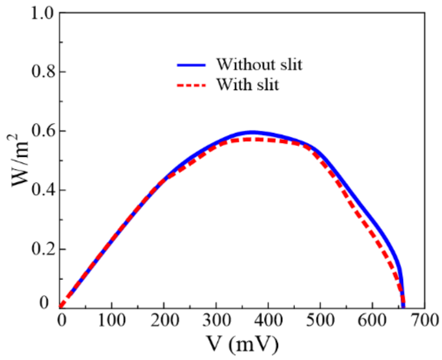

Fig. 19. Power curve characteristics of the solar cell with and without a slit.

V. Experimental Results

A prototype was constructed to validate the results of the designed wideband solar cell–integrated antenna, and it is depicted in Fig. 20. It can be seen in the figure that the inner conductor

Table 1. Performance comparison of the proposed design with existing solar cell antennas

Study	Size (λ_o^3)	BW (%)	Gain (dBi)	OT (%)	Rad. type	FF (%)
Liu et al. [8]	1.10 × 1.10 × 0.076	4	4.1	100	O	25
Zhao et al. [12]	1.6 × 1.2 × 0.024	15.5	8.5	100	U	51
An et al. [13]	1.10 × 1.32 × 0.22	52.1	9.8	100	U	12.5
O'Conchubhair et al. [19]	1.27 × 1.27 × 0.056	3.35	3.5	94.7	U	97.3
Ali et al. [27]	0.26 × 0.27 × 0.0054	31.4	2.8	100	O	90
Ali et al. [28]	0.408 × 0.204 × 0.0046	5.7	2.7	100	O	99.1
Proposed	0.38 × 0.15 × 0.0043	42.4	2.8	100	O	99.1

BW = impedance bandwidth, OT = optical transparency, FF = form factor, O = omni-directional, U = unidirectional.

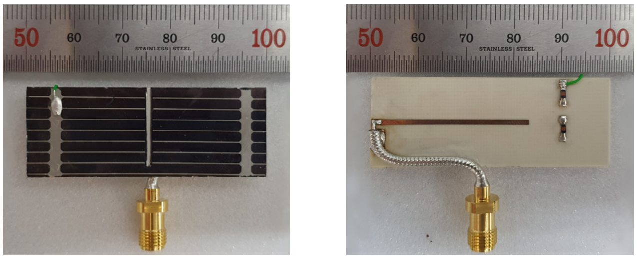

(a) (b)

Fig. 20. Fabricated prototype of the proposed antenna: (a) top view and (b) bottom view.

of SMA was connected to the microstrip feedline, while the outer conductor was connected to the small metallic patch to the ground plane using holes.

The reflection coefficient was measured using a Rohde and Schwarz ZVA67 network analyzer, while the radiation characteristics were measured using a full-wave anechoic chamber and an Agilent E8362B network analyzer. The full-wave anechoic chamber was 15.2 m (W) × 7.9 m (L) × 7.9 m (H). A standard wideband horn antenna was used for transmission, while the proposed solar cell–integrated antenna was used for reception. A comparison of the simulated and measured reflection coefficients of the proposed antenna is shown in Fig. 21. It can be seen from the figure that the measured reflection coefficient is in good agreement with the simulated results, and the impedance bandwidth of the measured results is nearly the same as in the simulations. The maximum measured gain was 2.84 dBi in the band of operation, and it is compared with the simulated gain in Fig. 22. Minor discrepancies between the simulated and measured gains were caused by fabrication and measurement errors. The simulated and measured normalized radiation patterns of the proposed solar cell–integrated antenna at 2.45 GHz are illustrated in Fig. 23. The proposed solar cell–integrated antenna has slightly directional radiation characteristics, as the

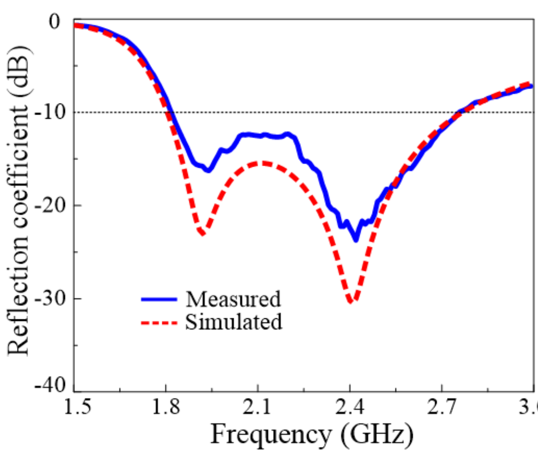

Fig. 21. Comparison of the measured and simulated reflection coefficients.

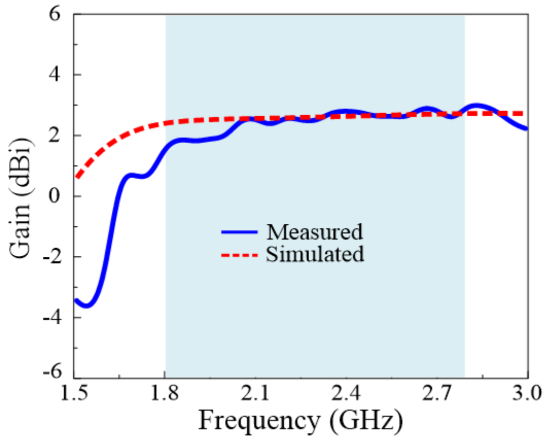

Fig. 22. Comparison of the measured and simulated gain.

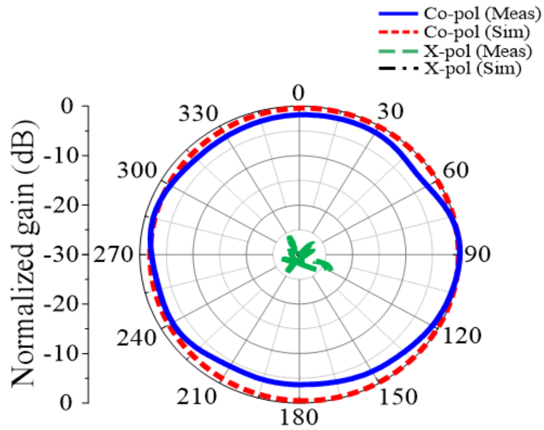

(a)

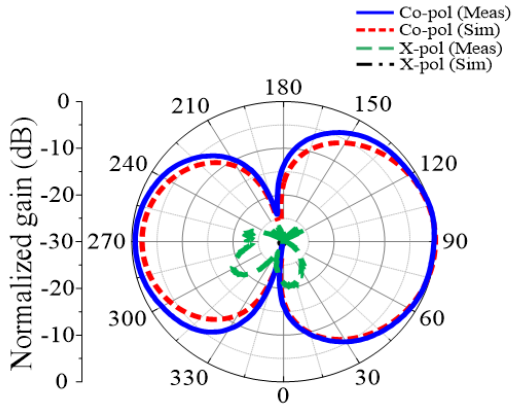

(b)

Fig. 23. Normalized radiation patterns of the proposed solar cell antenna at 2.45 GHz: (a) the H-plane and (b) the E-plane.

current is stronger on the x-axis direction than on the y-axis. Therefore, the antenna radiates in the direction of the stronger field. The comparison of the simulated and measured radiation patterns in Fig. 11 shows the similarity between the results. In addition, the experimental setup used to measure the radiation patterns of the proposed design is shown in Fig. 24.

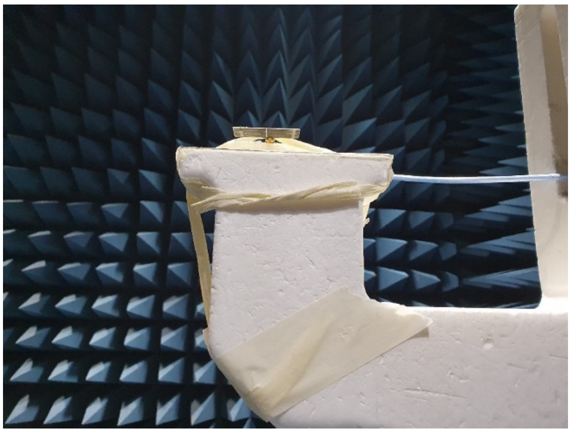

Fig. 24. Radiation pattern measurement setup.

VI. CONCLUSION

In this paper, we proposed a wideband ultra-low-profile solar cell–integrated antenna with a high form factor. A CIGS-based solar cell was also utilized as an antenna by cutting a slit into it. To increase the form factor, a very narrow slit of only 0.5 mm × 18 mm was used. The slit was fed by a coaxial-to-microstrip-line transition that was printed under the second substrate. An RF decoupler was also designed for use under the second substrate, so that the solar cells and the antenna work independently. The proposed solar cell–integrated antenna has a wide impedance bandwidth of 42.45% with a very compact size of 50 mm × 20 mm × 0.571 mm ($0.382\lambda_o \times 0.152\lambda_o \times 0.0043\lambda_o$ at 2.28 GHz) and a high form factor of 99.1%. Furthermore, the gain varied from 1.79 dBi to 2.84 dBi in the impedance bandwidth range. To validate the concept, a prototype was fabricated and measured, and the results were in close agreement with the simulated results.

This work was supported in part by the National Research Foundation of Korea (NRF) grant funded by the Korea government (MSIT) (No. NRF-2022R1F1A106 5324); in part by the National Research Foundation of Korea (NRF) grant funded by the Korea government (MSIT) (No. 2021R1A 4A1030775); in part by the Institute of Information & communications Technology Planning & Evaluation (IITP) grant funded by the Korea government (MSIT) (No. 2022-0-00704-001, Development of 3D-NET Core Technology for High-Mobility Vehicular Service), and in part by the Ajou University Basic Research Fund.

REFERENCES

[1] Y. Zhang, G. A. Vandenbosch, and S. Yan, "Low-profile broadband antenna with pattern diversity," *IEEE Antennas and Wireless Propagation Letters*, vol. 19, no. 7, pp. 1231-1235, 2020.

[2] Q. Zhang and Y. Gao, "A compact broadband dual-polarized antenna array for base stations," *IEEE Antennas and Wireless Propagation Letters*, vol. 17, no. 6, pp. 1073-1076, 2018.

[3] S. A. Haydhah, F. Ferrero, L. Lizzi, M. S. Sharawi, and A. Zerguine, "A multifunctional compact pattern reconfigurable antenna with four radiation patterns for sub-GHz IoT applications," *IEEE Open Journal of Antennas and Propagation*, vol. 2. pp. 613-622, 2021.

[4] L. Y. Nie, X. Q. Lin, B. Wang, and J. Zhang, "A planar multifunctional four-port antenna system for sub-urban mobile tablet," *IEEE Access*, vol. 7, pp. 56986-56993, 2019.

[5] V. T. Bharambe, J. Ma, M. D. Dickey, and J. J. Adams, "Planar, multifunctional 3D printed antennas using liquid metal parasitics," *IEEE Access*, vol. 7, pp. 134245-134255, 2019.

[6] S. X. Ta, J. J. Lee, and I. Park, "Solar-cell metasurface-integrated circularly polarized antenna with 100% insolation," *IEEE Antennas and Wireless Propagation Letters*, vol. 16, pp. 2675-2678, 2017.

[7] O. Yurduseven and D. Smith, "Solar cell stacked dual-polarised patch antenna for 5.8 GHz band WiMAX network," *Electronics Letters*, vol. 49, no. 24, pp. 1514-1515, 2013.

[8] S. Liu, D. Yang, Y. Chen, X. Zhang, and Y. Xiang, "Compatible integration of circularly polarized omnidirectional metasurface antenna with solar cells," *IEEE Transactions on Antennas and Propagation*, vol. 68, no. 5, pp. 4155-4160, 2020.

[9] A. Ali, H. Wang, Y. Yun, J. Lee, and I. Park, "Compact slot antenna integrated with photovoltaic cell," *Journal of Electromagnetic Engineering and Science*, vol. 20, no. 4, pp. 248-253, 2020.

[10] E. H. Lim, K. W. Leung, C. C. Su, and H. Y. Wong, "Green antenna for solar energy collection," *IEEE Antennas and Wireless Propagation Letters*, vol. 9, pp. 689-692, 2010.

[11] B. Xi, X. Liang, Q. Chen, K. Wang, J. Geng, and R. Jin, "Optical transparent antenna array integrated with solar cell," *IEEE Antennas and Wireless Propagation Letters*, vol. 19, no. 3, pp. 457-461, 2020.

[12] Y. Zhao, W. An, Y. Luo, S. Li, L. Xiong, and S. Yu, "Low-profile antenna integrated with solar cells for the 2.4 GHz band," *IEEE Antennas and Wireless Propagation Letters*, vol. 20, no. 4, pp. 443-447, 2021.

[13] W. An, L. Hong, Y. Luo, K. Ma, J. Ma, and X. Huang, "A wideband dual-function solar cell dipole antenna for both energy harvesting and wireless communications," *IEEE Transactions on Antennas and Propagation*, vol. 69, no. 1, pp. 544-549, 2021.

[14] R. Caso, A. D'Alessandro, A. Michel, and P. Nepa, "Integration of slot antennas in commercial photovoltaic panels for stand-alone communication systems," *IEEE Transactions on Antennas and Propagation*, vol. 61, no. 1, pp. 62-69, 2013.

[15] T. R. Jones, J. P. Grey, and M. Daneshmand, "Solar panel integrated circular polarized aperture-coupled patch antenna for CubeSat applications," *IEEE Antennas and Wireless Propagation Letters*, vol. 17, no. 10, pp. 1895-1899, 2018.

[16] S. Lemey, F. Declercq, and H. Rogier, "Dual-band substrate integrated waveguide textile antenna with integrated solar harvester," *IEEE Antennas and Wireless Propagation Letters*, vol. 13, pp. 269-272, 2014.

[17] S. X. Ta and I. Park, "A circularly polarized antenna integrated with a solar cell metasurface for CubeSat," in *Proceedings of 2018 Asia-Pacific Microwave Conference (APMC)*, Kyoto, Japan, 2018, pp. 696-698.

[18] W. An, S. Xu, F. Yang, and J. Gao, "A Ka-band reflectarray antenna integrated with solar cells," *IEEE Transactions on Antennas and Propagation*, vol. 62, no. 11, pp. 5539-5546, 2014.

[19] O. O'Conchubhair, P. McEvoy, and M. J. Ammann, "Integration of antenna array with multi-crystalline silicon solar cell," *IEEE Antennas and Wireless Propagation Letters*, vol. 14, pp. 1231-1234, 2015.

[20] S. X. Ta and I. Park, "A circularly polarized antenna integrated with metasurface solar cells," in *Proceedings of 2017 IEEE-APS Topical Conference on Antennas and Propagation in Wireless Communications (APWC)*, Verona, Italy, 2017, pp. 120-122.

[21] O. O'Conchubhair, K. Yang, P. McEvoy, and M. J. Ammann, "Amorphous silicon solar Vivaldi antenna," *IEEE Antennas and Wireless Propagation Letters*, vol. 15, pp. 893-896, 2015.

[22] J. Oh, K. Lee, T. Hughes, S. Forrest, and K. Sarabandi, "Flexible antenna integrated with an epitaxial lift-off solar cell array for flapping-wing robots," *IEEE Transactions on Antennas and Propagation*, vol. 62, no. 8, pp. 4356-4361, 2014.

[23] T. W. Turpin and R. Baktur, "Meshed patch antennas integrated on solar cells," *IEEE Antennas and Wireless Propagation Letters*, vol. 8, pp. 693-696, 2009.

[24] S. V. Shynu, M. J. Roo Ons, P. McEvoy, M. J. Ammann, S. J. McCormack, and B. Norton, "Integration of microstrip patch antenna with polycrystalline silicon solar cell," *IEEE Transactions on Antennas and Propagation*, vol. 57, no. 12, pp. 3969-3972, 2009.

[25] S. Zarbakhsh, M. Akbari, M. Farahani, A. Ghayekhloo, T. A. Denidni, and A. Sebak, "Optically transparent subarray antenna based on solar panel for CubeSat application," *IEEE Transactions on Antennas and Propagation*, vol. 68, no. 1, pp. 319-328, 2020.

[26] S. K. Podilchak, D. Comite, B. K. Montgomery, Y. Li, V. G. G. Buendia, and Y. M. M. Antar, "Solar-panel integrated circularly polarized meshed patch for CubeSats and other small satellites," *IEEE Access*, vol. 7, pp. 96560-96566, 2019.

[27] A. Ali, Y. Yun, H. Wang, K. Lee, J. Lee, and I. Park, "Photovoltaic cell with built-in antenna for internet of things applications," *IEEE Access*, vol. 9, pp. 107437-107445, 2021.

[28] A. Ali, H. Wang, J. Lee, Y. H. Ahn, and I. Park, "Ultra-low profile solar-cell-integrated antenna with a high form factor," *Scientific Reports*, vol. 11, article no. 20918, 2021. https://doi.org/10.1038/s41598-021-00461-w

Ahmed Ali

received his M.S. degree in electrical engineering with a specialization in telecommunication engineering from COMSATS University Islamabad, Attock, Pakistan, in 2019. He is pursuing his Ph.D. degree in the Department of Electrical and Computer Engineering at Ajou University, Suwon, Republic of Korea. His current research interests include developing metasurface antennas and photovoltaic cell–integrated antennas for IoT applications.

Heesu Wang

received his B.S. and M.S. degrees in electrical and computer engineering from Ajou University, Suwon, Republic of Korea, in 2018 and 2020, respectively. He is currently studying for his Ph.D. degree at the Department of Electrical and Computer Engineering at Ajou University. His research interests include the design of patch antennas, printed antennas, small antennas, and metasurface antennas for various wireless communication applications.

Yeojun Yun

received his B.S. degree in electrical and computer engineering from Ajou University, Suwon, Republic of Korea, in 2014. He is currently studying for his Ph.D. degree in the Department of Electrical and Computer Engineering at Ajou University. His research interests include the design of flexible III–V photovoltaic cells, high-quality periodic nanostructures, and fabrication processes for flexible optoelectronic nanodevices.

Sungjun Park

received his Ph.D. degree from the School of Materials Science and Engineering at Gwangju Institute of Science and Technology, Gwangju, Korea, in 2016. He worked as a post-doc in RIKEN, Wako, Japan, from 2016 to 2018 and as a Senior Researcher at Samsung Advanced Institute of Technology (SAIT) Suwon, Korea, from 2018 to 2020. He then joined the Department of Electrical and Computer Engineering, Ajou University, Suwon, Republic of Korea, where he is an Assistant Professor. His current research interests include flexible and stretchable electronics for wearable and bio-medical applications.

Yong Bae Park

received his B.S., M.S., and Ph.D. degrees in electrical engineering from the Korea Advanced Institute of Science and Technology, Republic of Korea, in 1998, 2000, and 2003, respectively. From 2003 to 2006, he was with the Korea Telecom Laboratory, Seoul, Republic of Korea. He joined the School of Electrical and Computer Engineering, Ajou University, Republic of Korea, in 2006, where he is currently a professor. His research interests include electromagnetic field analysis, high-frequency methods, metamaterial antennas, radomes, and stealth technology.

Jaejin Lee

received his B.S. and M.S. degrees in physics education from Seoul National University, Republic of Korea, and his Ph.D. degree in electrical engineering from the Northwestern University, USA. He is currently a Professor in the Department of Electrical and Computer Engineering at Ajou University, Suwon, Republic of Korea. He was a Visiting Scholar in the Department of Electrical and Computer Engineering at the University of Wisconsin at Madison, USA. His research interests include the metalorganic chemical vapor deposition (MOCVD) growth of III–V com-pound semiconductor heterostructures, high-efficiency III–V solar cells, LEDs, and semiconductor diode lasers. He has authored and co-authored more than 100 refereed journal articles and conference papers. He holds more than 20 patents.

Ikmo Park

received his B.S. degree in electrical engineering from the State University of New York at Stony Brook, and his M.S. and Ph.D. degrees in electrical engineering from the University of Illinois at Urbana-Champaign. He joined the Department of Electrical and Computer Engineering at Ajou University in 1996. Before joining Ajou University, he worked in the Device & Materials Laboratory of LG Corporate Institute of Technology, Seoul, Republic of Korea, where he had been engaged in research and development of various antennas for personal communication systems, wireless local area networks, and direct broadcasting systems. He was a Visiting Professor at the Department of Electrical and Computer Engineering, POSTECH, Pohang, Republic of Korea, from March 2004 to February 2005, and the Department of Electrical and Computer Engineering, University of Arizona, Tucson, Arizona, USA, from July 2011 to June 2012. He has authored and co-authored more than 400 technical journal and conference papers. He also holds over 50 domestic and international patents. He served as a Chair of the Department of Electrical and Computer Engineering at Ajou University. He is a member of the Board of Directors at the Korea Institute of Electromagnetic Engineering and Science (KIEES). He serves as the Editor-in-Chief of the Proceedings of the KIEES and Journal of KIEES, is an Editorial Board member of the International Journal of Antennas and Propagation, and is an Associate Editor of IET Electronics Letters. He has also served as an Editorial Board member of the Journal of Electromagnetic Engineering and Science. He is a member of Eta Kappa Nu and Tau Betta Pi.